Redesigning a Moving Magnet Transducer for Use in a Low-Profile Home Speaker

Brandon Cote

bwcote@wpi.edu

A Major Qualifying Project submitted to the faculty of
Worcester Polytechnic Institute
in partial fulfillment of the requirement for the
Degree in Bachelor of Science in Mechanical Engineering

Submitted To:
Professor Joe Stabile, Worcester Polytechnic Institute

Table of Contents

Abstract

The objective of this project was to improve upon the existing design of previous Major Qualifying Projects and create a functioning prototype of a moving magnet transducer which could drive speaker cones in a low-profile enclosure. This project began by examining the existing build of the previous year's motor assembly and performing root cause analyses to determine its points of failure to improve upon. The motor assembly was redesigned and prototyped to provide optimum functionality and reliability, with recommendations for future improvements. The motor was also tested for force versus current analyses to determine the expected force output for sound production.

Acknowledgements

This project was impacted by many individuals and organizations outside of the project group which we would like to extend our gratitude to. Firstly, we would like to give thanks to Professor Joe Stabile, our advisor and mentor on the project. The vision for our project came from Professor Stabile; He was very engaging with the technical aspects of the project and proved to be the best resource on the subject. He always invested his time and personal effort to encourage the success of the project. We would also like the thank the WPI Mechanical Engineering Department, the WPI 3D Printing Laboratory, the WPI Makerspace, and other organizations who offered the essential resources for experimentation. Lastly, we would like to thank Worcester Polytechnic Institute for allowing us the freedom to work on a unique technical project. It has been an experience which has delivered important skills combining electrical and mechanical engineering disciplines.

List of Figures

List of Tables

Executive Summary

The goal of this project was to continue the work of previous Major Qualifying Projects to build a functioning moving magnet transducer that could drive speaker cones in a low-profile enclosure. After analyzing the existing motor assembly, it was evident that it was not functioning as intended due to possible issues with tolerances and structural integrity of the materials which housed the lever and electromagnetic stators. We examined each part of the existing motor

assembly to troubleshoot the visible issues with the motor and discovered fit and tolerance issues among the small mechanical parts connecting the lever to the PLA motor fixture. We also discovered lacking structural integrity in some PLA parts and the PLA fixture. We created a plan on how to begin redesigning the motor to operate as intended in previous years MQP's, which first involved investigating the existing modes of failure for the assembly. Throughout the course of this project, the motor assembly was redesigned, fabricated, and tested for optimum reliability and strength a series of times. By the end of the project, the motor assembly could operate with the stators and magnets aligned optimally and produce sufficient force for sound production. Additionally, a test fixture was constructed to perform physical analyses on the motor assembly which could record force vs. current output at the cone. We built multiple iterations of this test assembly to ensure accuracy and ease of operation and performed tests under a variety of different conditions to understand the performance of the motor.

1.0 Background

Speakers produce sound by driving cones, which are often a planar area attached to flexible surrounds allowing for movement along one axis. When driven, these cones vibrate and pressurize the air around them, creating waves which we hear as sound (Wykes, 2022). Most modern speakers drive their cones with a voice coil, or electromagnetic coil placed within the speaker's enclosure. This coil is free to move axially. It sits within a magnet that is fixed within

the enclosure and is attached to a cone on one end. When the voice coil of the speaker is supplied with current from an amplifier, an electromagnetic field is created within the voice coil that interacts with the magnetic field of the fixed magnet. This is what drives the cones and creates sound. Cones can also be driven to produce sound using a motor such as a moving magnet transducer (MMT). These motors operate very similarly to voice coil, however with an MMT, the stator is fixed while the magnets are free to move and drive the cones. With an MMT, there are many different configurations which allow for the force of the moving magnets to be transferred from the magnets to the cones. In all configurations, it is necessary for there to be proper spacing and alignment between the electromagnetic stators and magnets to "ensure proper operation" of the motor (Pance, 2014). MMT's are specifically chosen for bass speakers because magnets often provide more moving mass than voice coils, therefore allowing for operation at lower bass frequencies given the equation (Roy, 2018):

$$wd = sqrt(\frac{k}{m} - \frac{b^2}{4m^2})$$

Previous Major Qualifying Projects (MQP's) have explored using an e-core transformer as a fixed electromagnetic driving a magnet and cone (Roy, 2018). An MQP in 2020 began experimenting with prototypes featuring a magnetic lever operated by two fixed electromagnetic stators (Ahrens, 2020). This idea was expanded upon in 2021, and 2022, and was to be further evolved as the scope of this project.

2.0 Redesigning the Motor Assembly

2.1 Evaluating Previous Motor Assembly Prototypes

This project was a continuation of work from previous years, therefore our first efforts involved examining the previous year's prototypes. This allowed us to better understand the desired functionality of the motor assembly and enclosure. Initially, Professor Stabile had informed us that the motor used to drive the cones was "crashing," and that the speaker enclosure itself was not airtight. Upon our analysis of the motor, we were able to confirm that it was not functioning properly. The entire assembly of the motor consisted of two moving magnet

transducers operating magnets within a lever meant to drive two opposing cones simultaneously. Both the moving magnet transducers and lever were mounted on a 3D printed motor fixture which could fasten to the inside of the enclosure. Reference figures 1, 2, and 3 for visuals of the previous motor assembly. It was quickly evident that the steel stators were slipping through their mounts due to lack on clamp force, and the lever was not strong enough to resist lateral bending, both due to the strong magnetic force between the magnets and stators. This was causing the magnets and stators to contact each other, resulting in the motor "crashing." When examining the enclosure, we first noticed that it had been sealed with a putty material around its seams, where external panels were mounted and in fastener locations. This putty seemed to lack proper sealing characteristics as it was not placed within the seams but rather coated along the outsides of them.

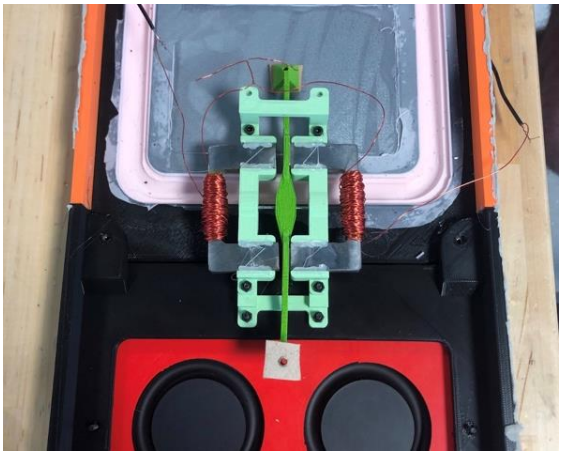

Figure 1: Image of Previous Motor Assembly

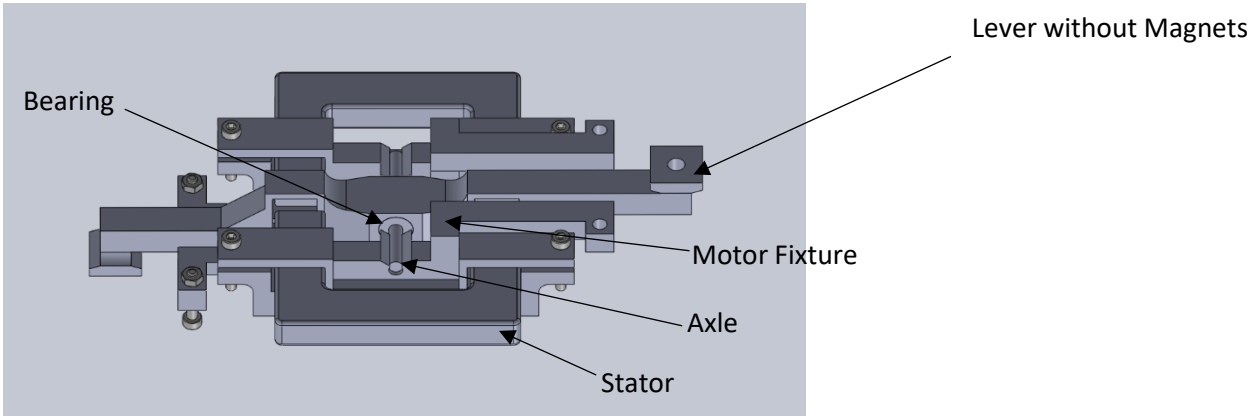

Figure 2: SolidWorks Model of Previous Motor Assembly

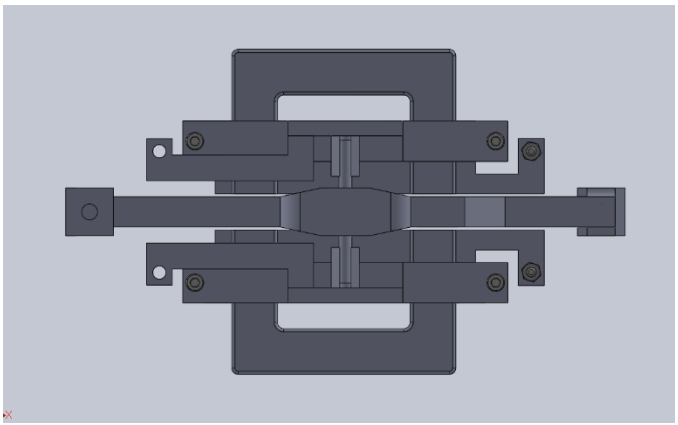

Figure 3: Top View of SolidWorks Model of Previous Motor Assembly

2.2 Iterating Previous Motor Assembly

Before deciding how to iterate the previous motor assembly, it was necessary to gain an understanding of its physics. We created diagrams detailing the correct orientation of stators and lever magnets in the motor assembly. This helped us to understand how magnetic flux travels through the stators and what orientation the lever magnets should be in so that the lever actuates in the desired direction with maximized force magnitude when current is applied. Using the right-hand rule, if the fingers are wrapped around the stator in the direction which current flows, then the north end of the stator is where the thumb points. Electromagnetic flux then flows between the two stators and travels from north to south, causing attraction between the now polarized stators and magnets in the lever arm. Alligator clips were installed on the leads of both stators so that current direction could be optimized, and concepts applied in the diagrams could be tested for accuracy. Magnet orientation could then be determined using compass and hall effect sensor, then marked with sharpie before installation. Figure 4 shows how flux travels through the electromagnetic stators from south to north when current is applied. Figure 5 shows how the lever arm actuates in response to applied current.

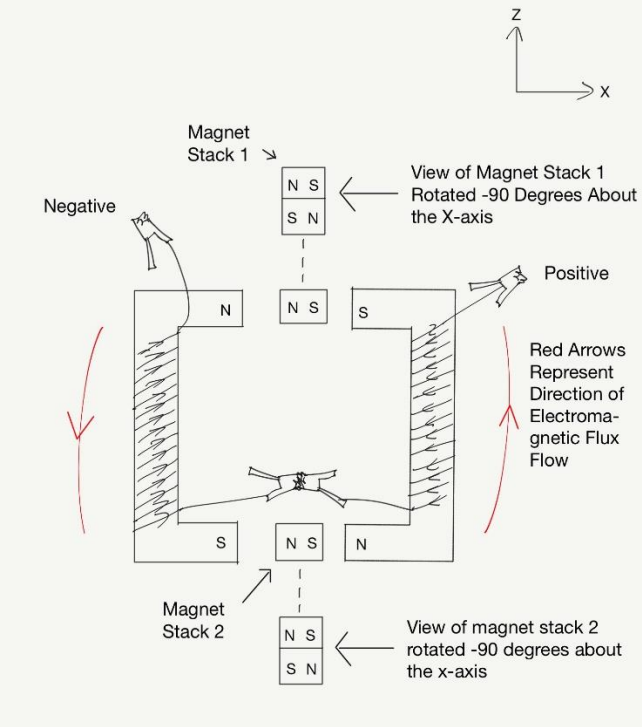

Figure 4: Orientation of Stators and Lever Magnets

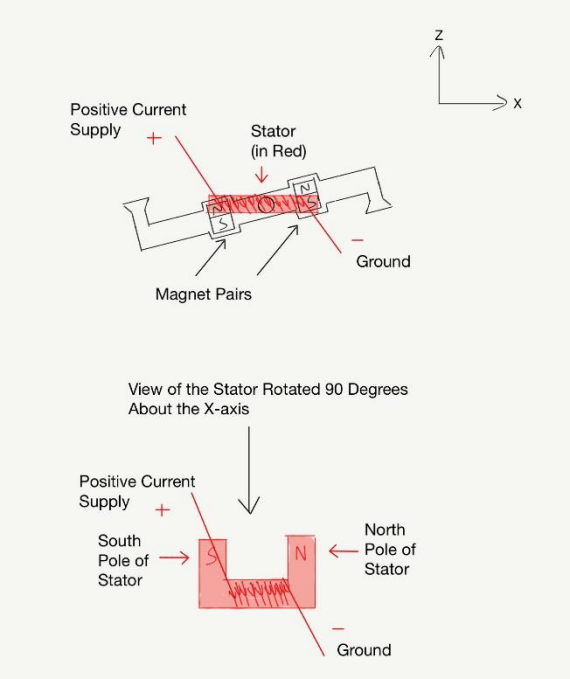

Figure 5: View of One Side of Lever Arm and One Stator (Actuated with Current)

It should be noted that the redesign of the motor assembly was always intended to preserve the cone spacing designated in last year's MQP. Once we understood the mechanics of the motor assembly it was easier to consider different ways to iterate and improve upon it, as

well as perform a more in-depth root cause analysis on its failure modes. It was immediately evident that there were many tolerances in the system which could cause motor to fail, including the stator clamps, axle parts, motor fixture, lever, and magnets. Therefore, each individual part of the assembly was modified to provide tighter tolerances and prevent unwanted movement of parts.

The motor fixture is the 3D printed model which contains the clamps for the stators and mounting point for the lever. The clamps for the stators consisted of a flange with one fastening point which could be tightened to increase clamping force (See figure 6). We were able to determine that the clamp flanges did not provide sufficient clamping force onto the stators, which was causing them to slide through the clamps into the lever magnets. The thin profile of the flanges combined with the one point of fastening on the far end of the flanges resulted in them bowing over the top of the stators (See figure 7). This meant that the clamp only contacted the top edges of the stators instead of creating an even pressure distribution over the stator's topsides.

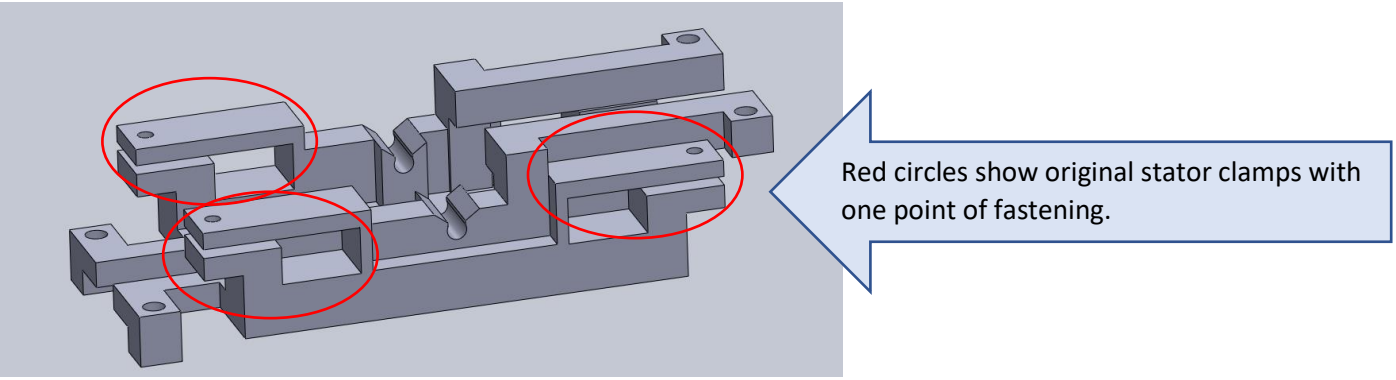

Figure 6: SolidWorks Model of Motor Fixture with Stator Clamp Flanges Circled

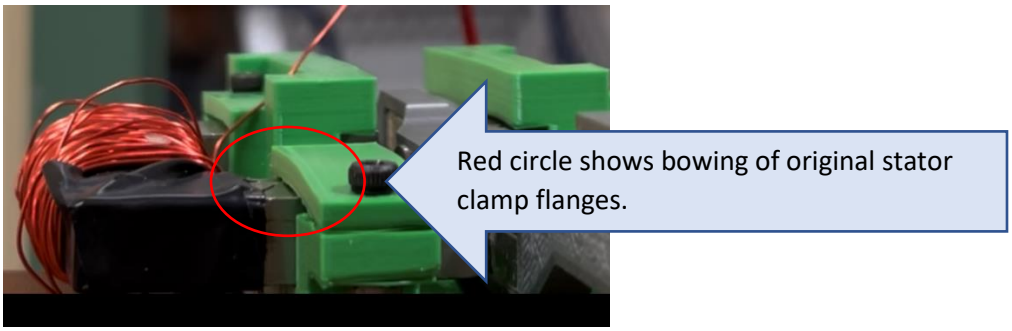

Figure 7: Clamp Flange Bowing Over Stator

To fix this issue, the original clamps were discarded, and the fixture was redesigned to accommodate stand-alone clamp flanges with two points of fastening. In figure 8 you can see the removal of the clamp flanges from the original motor fixture, while figure 9 shows the addition

of hardware recesses on the bottom of the fixture to accommodate the extra 4 required fasteners. This involved creating and mirroring 8 cut extrusions and 6 boss extrusions to preserve the integrity of the top enclosure mounting brackets and the dimensions of the recesses for the stators.

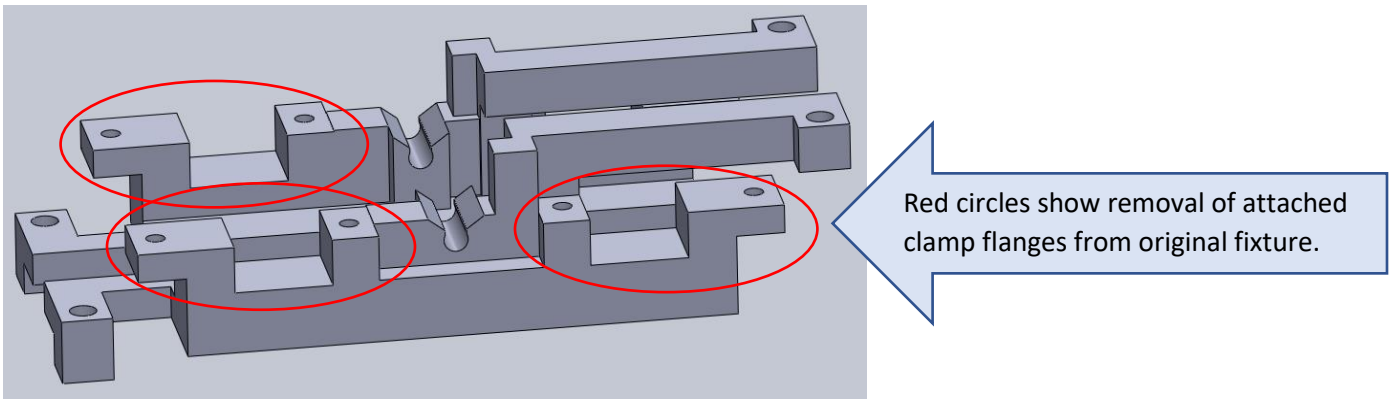

Figure 8: Removal of Clamp Flanges from Previous Motor Fixture

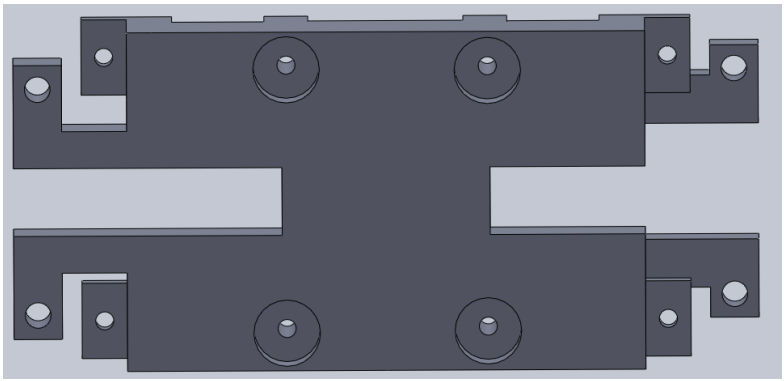

Figure 9: Recesses on Bottom of Motor Fixture for Added Fasteners

The stand-alone clamp flanges were designed separately from this model, and the original iteration of them can be seen in figure 10. These clamp flanges and the model in figure 8 were printed in the Makerspace and the motor assembly was rebuilt with these parts and the pre-existing lever, magnets, axle, bearings, bearing spacers, and stators. Upon rebuilding, it was confirmed the stators could now be adequately clamped into the motor fixture without creeping over time. The model in figure 8 was saved as a file called “2022 Motor Fixture 1.0,” while the model in figure 10 was saved as “Clamp Flanges 1.0.”

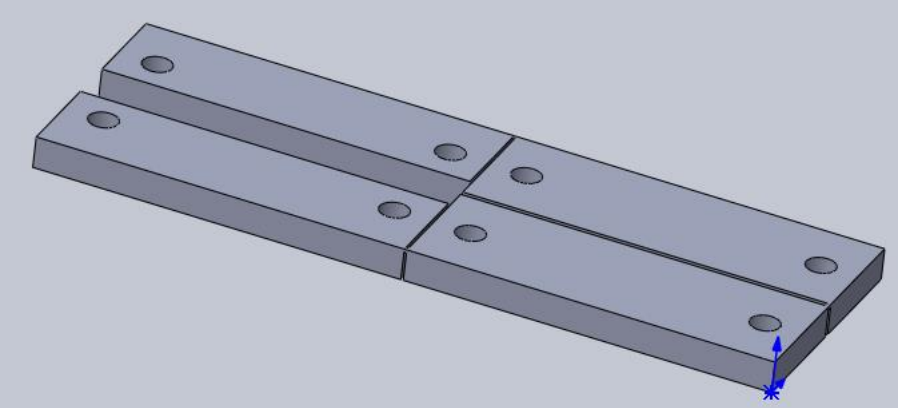

Figure 10: Stand-Alone Clamp Flanges

With the variable of crashing stators eliminated, the root cause analysis continued, and the following factors were determined to contribute to the ongoing crashing of the motor assembly.

1. Tolerance between motor fixture axle mounts and axle itself too large.

2. Tolerance between outer diameter of bearings and bearing recesses in lever arm too large

3. PLA spacer width too small to provide sufficient preload on radial bearings

4. Profile of lever arm too thin to remain rigid against electromagnetic force

These factors were derived largely from visual analysis of the motor assembly, overall feel of play in parts, and evidence of stress fracturing and yielding in some areas of parts.

The first issues to be addressed were the tolerances between the lever axle and axle mounts in the motor fixture being too large. These tolerances were tightened by reducing the diameter of the axle hole/mount by 0.01 inches. This resulting diameter is 0.004 inches smaller than the diameter of the axle in use, which was measured to be 0.155in using a dial caliper. Additionally, the walls between the top opening of the axle mount were reduced from 0.07 to 0.0675 inches to accommodate the new diameter, and the “V-Cut” dimensions were changed as well. The “V-Cut” and top-down installation method was retained from the previous model for ease of lever arm removal and experimentation. These tolerance changes resulted in a much tighter axle fit with no visible play. Figure 11 shows the original dimensions of the axle mounting holes while figure 12 shows the updated dimensions of the axle mounting holes. Figure 15 shows the exploded location on the motor fixture where these changes occurred.

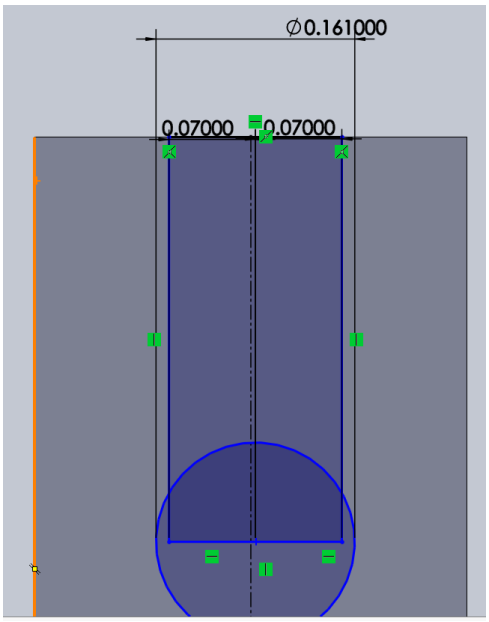

Figure 11: Original Dimensions of Axle Mounting Holes

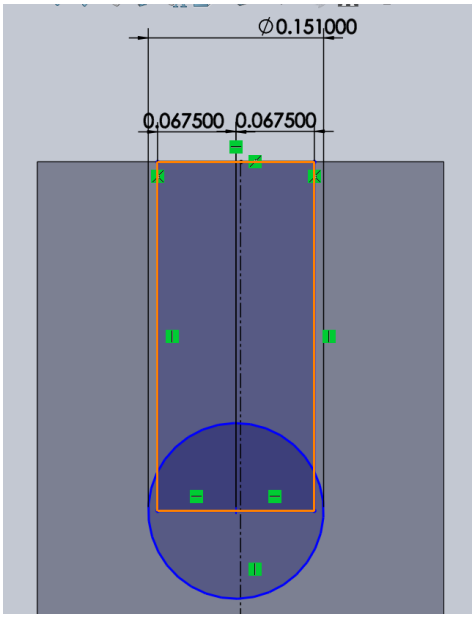

Figure 12: Updated Dimensions of Axle Mounting Holes

Additionally, Figure 13 shows the original dimensions of the v-cut on the axle mount. This v-cut was kept because it allows the hole in the axle mount to act as a snap ring and retain the axle through a top-down installation method. Figure 14 shows the updated dimensions of the v-cut to accommodate the tighter axle mounting hole and increase the level of force holding in

the axle. An expanded view showing the location these changes occurred is shown in Figure 15. The motor fixture was resaved as a file called “2022 Motor Fixture 2.0.”

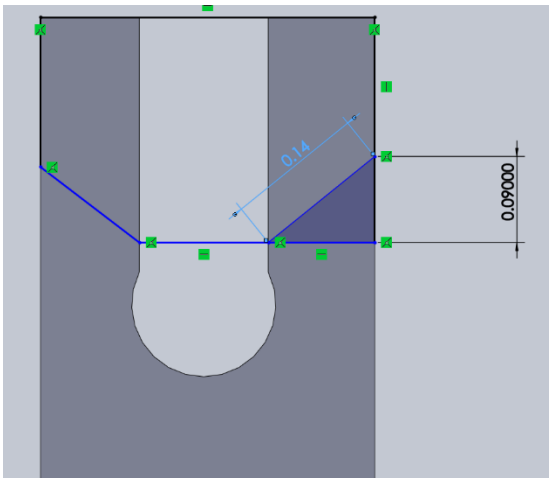

Figure 13: Original Dimensions of the V-Cut on the Axle Mounts

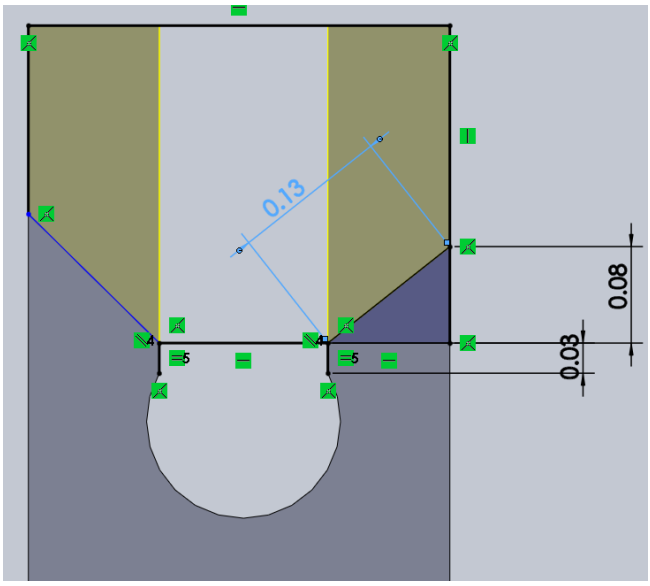

Figure 14: Updated Dimensions of the V-Cut on the Axle Mounts

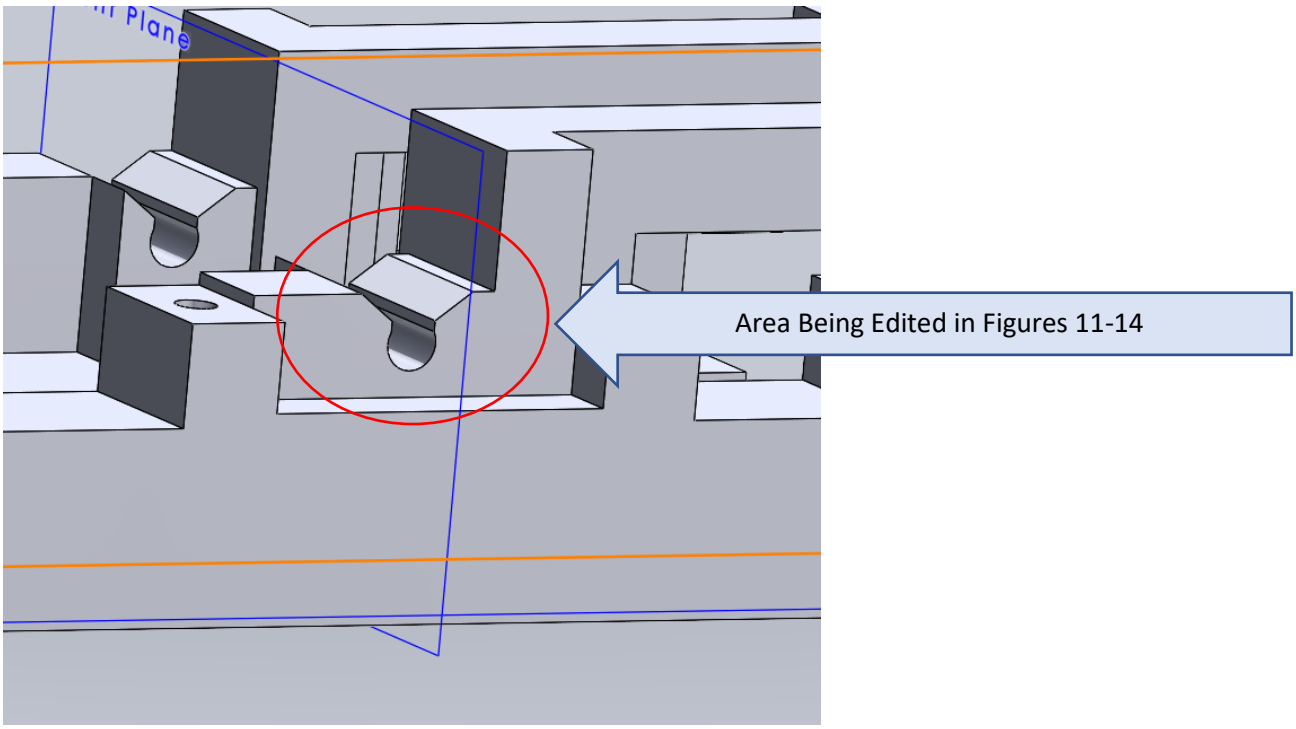

Figure 15: Exploded View of Updated Axle Mounts

The next step was to address the large tolerance between the radial flange bearings and the recesses of the lever arm itself. This was determined to be an issue with the previous design when noticeable play was seen between the two parts. To tighten these tolerances, the diameter of the sketch for the bearing recess on the center of the lever arm was reduced by 0.02 inches. This proved to be sufficient as installation of the bearings now required forceful insertion utilizing soft taps from a rubber mallet. This ensured there would be no movement of these bearings in the lever arm body. Figure 16 shows the original dimensions of the bearing recess in the lever arm, while Figure 17 shows the updated dimensions. The outside diameter of the bearings in use were measured at 0.40 inches, therefore the new dimensions provided an interference fit between the lever and bearings.

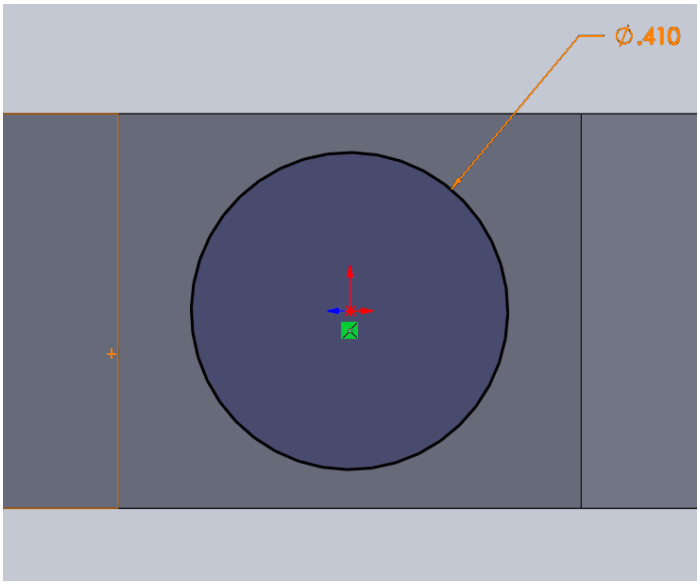

Figure 16: Original Dimensions of Lever Arm Bearing Recess

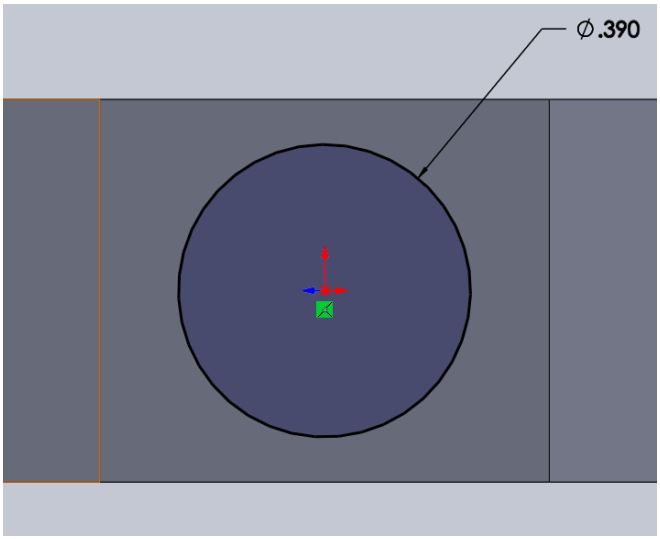

Figure 17: Updated Dimensions of Lever Arm Bearing Recess

The third issue addressed was the dimensions of the PLA spacers used between the motor fixture axle mounts and lever bearings. The original spacers were noticeably thin and did not adequately apply pressure to the inner race of the flanged bearing, creating opportunity for side-to-side and angular play of the lever arm. The required dimensions of the spacers were measured using a dial caliper, however the effects of compression on the PLA spacer once installed were unknown. Therefore, a total of four bearing iterations were designed and printed to install and test.

A dial caliper was used to measure a needed spacer height of 0.125in to properly fill the gap between bearings and motor fixture. To create an interference fit, spacers with heights of 0.135in and 0.145in were printed. Bearings with these heights were iterated with both 0.155in

I.D. and 0.23in O.D. and 0.16in I.D. and 0.24in O.D. to see which would better fit the axle due to inconsistencies in PLA prints. See the white boxes in figures 18-20 for detailed dimensions of each iteration. The spacers with the best fit were 0.16 I.D., 0.24in O.D., and 0.135in height, which added sufficient preload to the bearings, eliminating almost all the side-to-side and angular play. The spacers were added onto the original "Clamp Flanges 1.0" file so that they could be printed simultaneously with a larger piece.

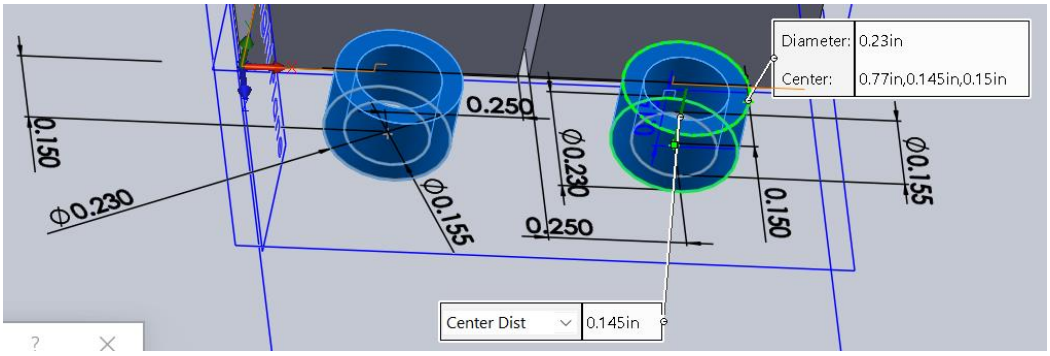

Figure 18: Spacer Iteration with 0.145in Center Distance (Height), 0.155in I.D, 0.23in O.D

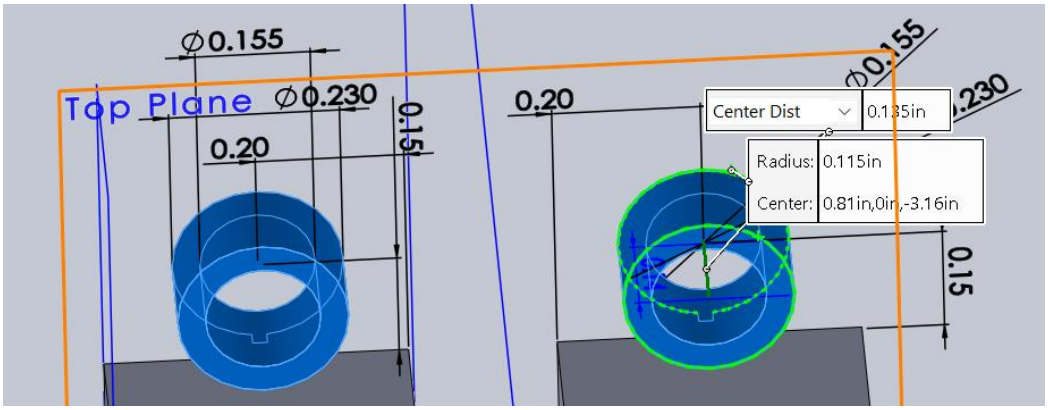

Figure 19: Spacer Design with 0.135in Center Distance (Height), 0.155in I.D, 0.23in O.D.

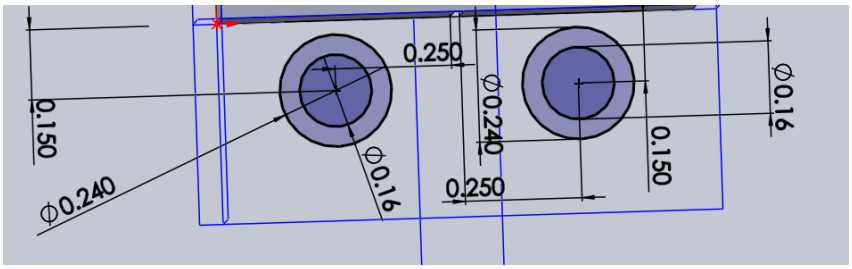

Figure 20: Altered Sketch with 0.16in I.D and 0.24in O.D.

Next, we determined that the thicknesses of the lever arm and the frame for the magnet recess in the lever were not large enough to remain rigid against the magnetic forces subjected to them. The profile of the lever arms was therefore increased from 0.25 inches to 0.34 inches to add rigidity and stability when subject to large electromagnetic forces. This decision was made considering the need for additional rigidity while needing to retain proper clearance throughout the path of the lever. Additionally, the thickness of the frame for the magnets was increased by 0.06in around the entire perimeter as its original profile was likely contributing to the flexion in the lever arms. This new design proved to be much stronger in the assembly and no longer exhibited excessive flexion. Figure 21 shows the original dimensions of the lever profile in SolidWorks while Figure 22 shows the updated dimensions. The new lever was saved as a SolidWorks file called "2022 New Lever 1.0."

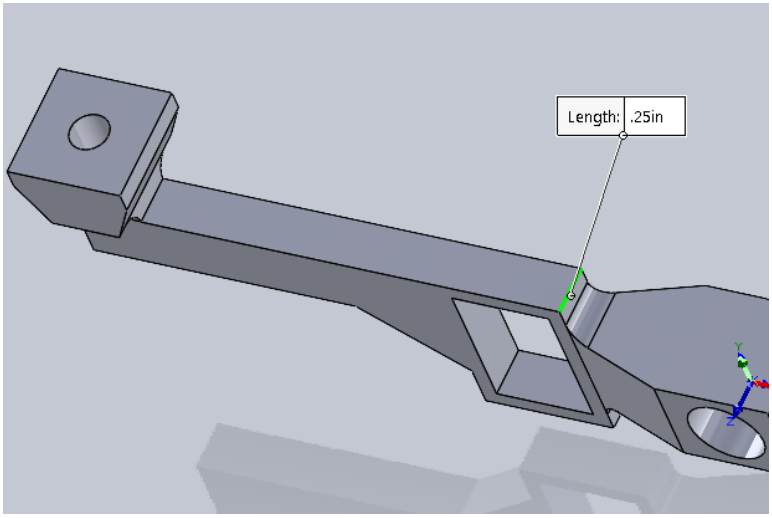

Figure 21: Original Width of Lever Profile (0.25 Inches)

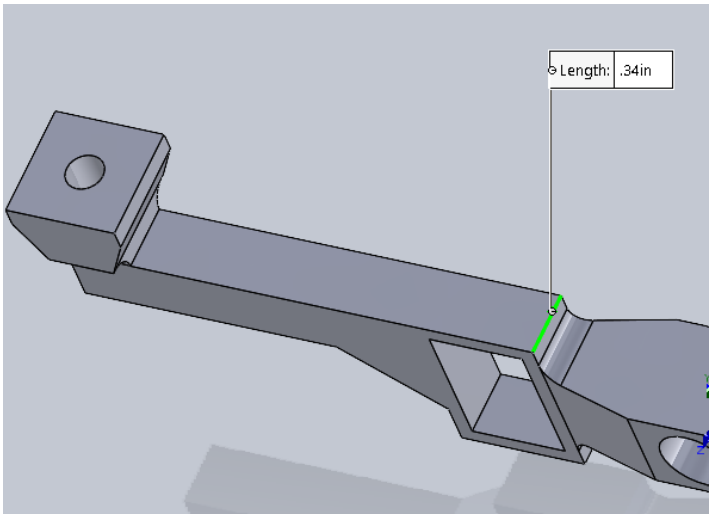

Figure 22: Updated Width of Lever Profile (0.34 Inches)

Additionally, Figure 23 shows the original dimensions of the magnet frame, while Figure 24 shows the updated dimensions.

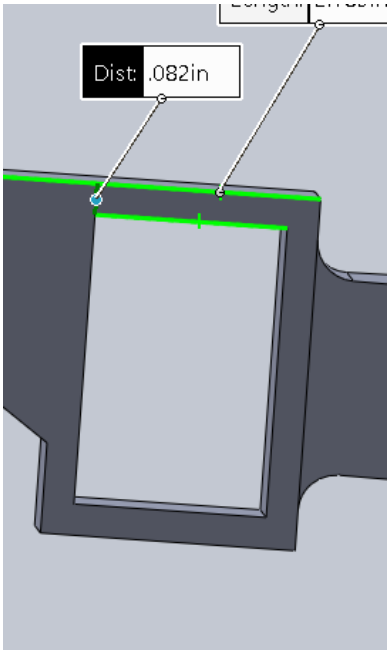

Figure 23: Original Width of Magnet Frame (0.082 Inches)

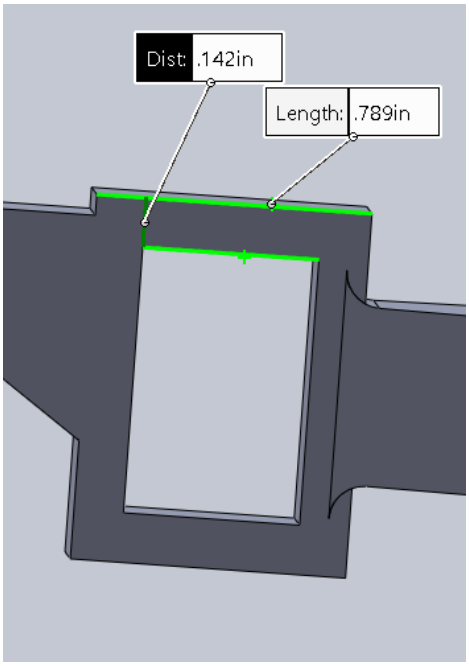

Figure 24: Updated Width of Magnet Frame (0.142 Inches)

The updated motor fixture (Figure 25), spacers and lever (Figure 26) were printed and assembled with the other existing parts.

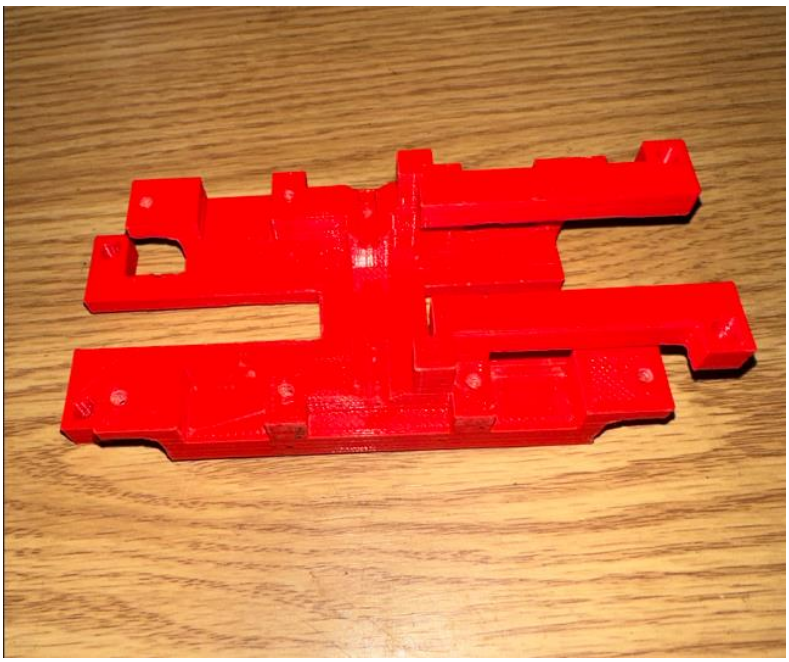

Figure 25: 3D Print of "2022 Motor Fixture 2.0"

Figure 26: 3D Print of "New Lever Arm 1.0" and Spacers from "Clamp Flanges 1.0" Print

After each of these changes were implemented, the motor fixture, lever, clamp flanges and spacers were printed and rebuilt into an assembly. It was found that the system still crashed when the stators got within 1mm of the magnets. With all variables considering axle, lever and bearing tolerance having been reduced, we resorted to examining the integrity of the motor fixture as a possible cause.

Ideally, the lever arm will always be perfectly centered between the stators and will never be drawn to one stator more than the other. The reality, however, is that as the lever actuates, its arms will naturally drift slightly off center due to the flexible nature of PLA material and the many tolerances in the system. This causes the magnets in the lever arm to have a higher attraction to one of the stators, because it is now physically closer to one of them when the lever drifts off center. This puts the lever arm in a state of force un-equilibrium since the force acting on one side of the arm will be greater than the force on the other side, so the naturally the lever arm will try to move towards the stator it has the greatest attraction to per the laws of physics.

Since the tolerance between bearings, axle, and motor fixture had all been reduced to very minimal amounts, we discovered that the motor fixture was compensating for this force un-equilibrium by torquing the very weak bridge in the center of the motor fixture until the magnet and stator touched and the system "crashed". The force balance was then in equilibrium. We figured a tougher bridge may apply enough resistive force so that the opposite forces acting on the lever arm would reach equilibrium long before crashing occurred.

The height and width of the motor fixtures bridge was increased, and the new motor fixture no longer exhibited torsional failure as predicted. Figure 27 shows a SolidWorks model displaying the original width of the motor fixture bridge, while Figure 28 shows the updated width. Figure 29 shows a SolidWorks model displaying the original height of the motor fixture bridge and Figure 30 shows the updated height.

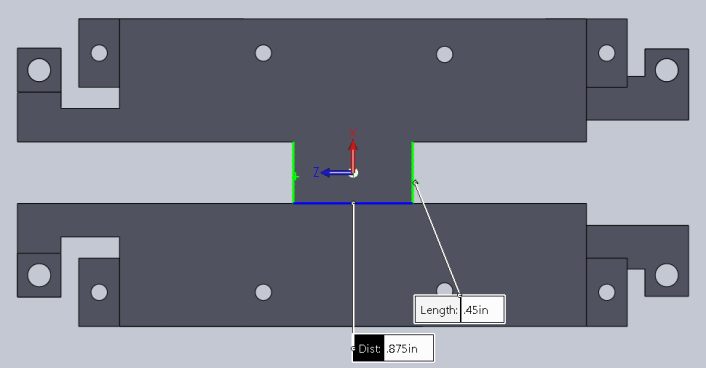

Figure 27: SolidWorks Model Displaying Original Width of Motor Fixture Bridge (0.875 Inches)

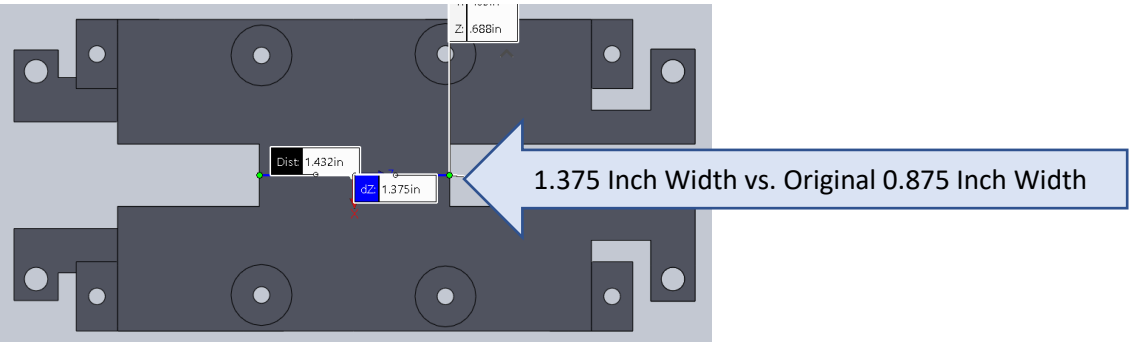

Figure 28: SolidWorks Model Displaying Updated Width of Motor Fixture Bridge (1.375 Inches))

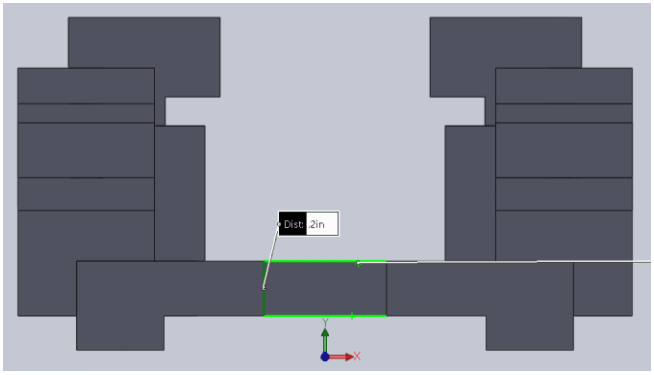

Figure 29: SolidWorks Model Showing Original Height of Motor Fixture Bridge (0.2 Inches)

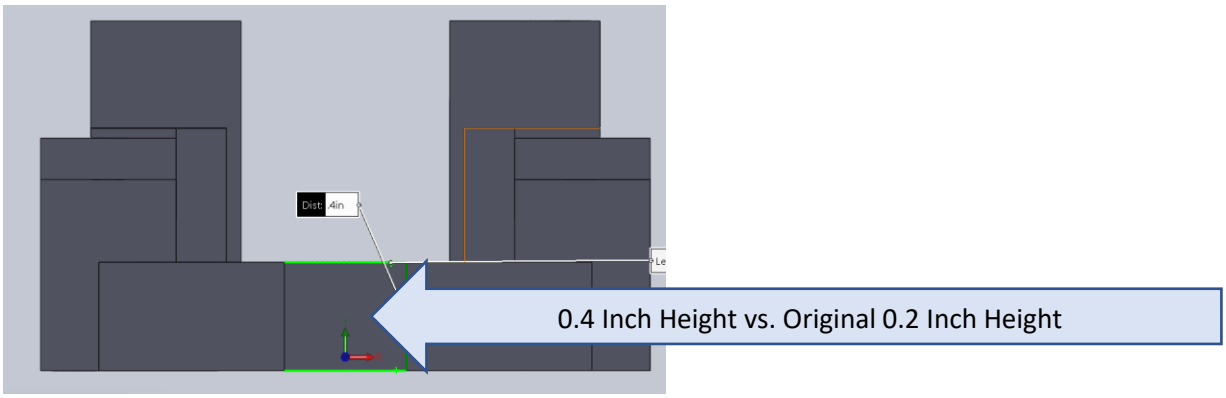

Figure 30: SolidWorks Model Showing Updated Height of Motor Fixture Bridge

When choosing these new dimensions, we considered how the motor fixture bridge would limit the maximum deflection angle of the lever. After talking with Professor Stabile, we understood the at least 5 millimeters of 0.197 inches of cones movement would be necessary to drive sound. Given these considerations the motor fixture bridge was redesigned to accommodate a deflection angle of up to 8 degrees. Figure 31 shows the dimensions of the lever in respect to the motor fixture which were used to calculate the allowable length of the motor fixture bridge.

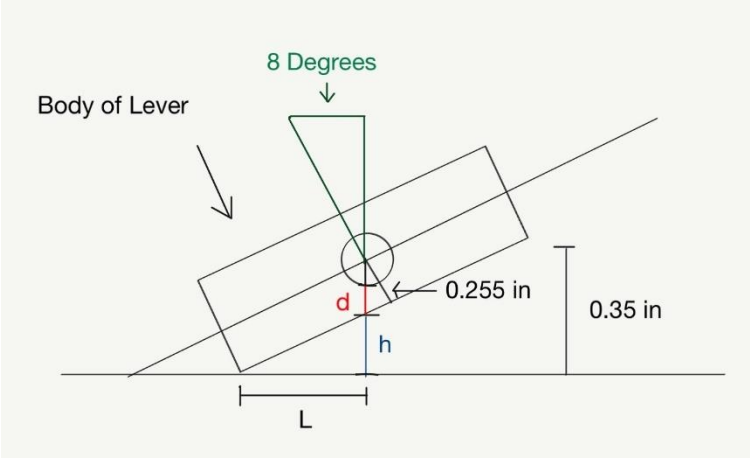

Figure 31: Dimensions Used to Calculate New Length of Motor Base

The calculations for L are as follows:

$$d = \frac{0.255\ inches}{\cos(8)} = 0.258\ inches$$

Therefore:

$$h = 0.35\ inches - 0.258\ inches = 0.092\ inche$$

And:

$$L = \frac{h}{\tan(theta)} = \frac{0.092\ inches}{\tan(8)} = 0.654\ inches$$

As a result, the length of the motor bridge was updated to 2*L, or 1.31 inches. Additionally, the amount of deflection achievable at the cones, X, was found using the following equation:

$$X = \tan(theta) * La$$

Where La = the length of one arm of the lever, measured as 3.1695 inches (Figure 32), therefore:

$$X = \tan(8) * (3.1695\ inches) = 0.445\ inches = 11.3\ millimeters$$

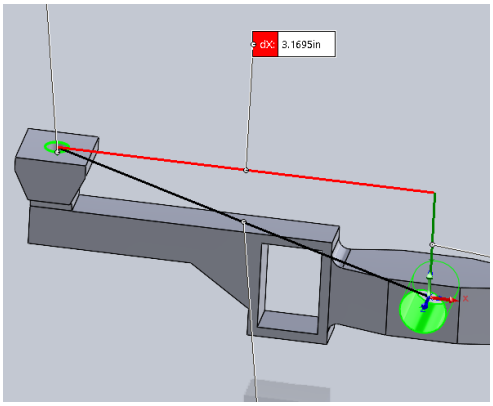

Figure 32: Length of One Arm of Lever (3.1695 Inches)

After changing the dimensions of the motor fixture bridge, we also had to readjust the position of the axle mounts on the motor fixture so that the axle would still lie centered in the fixture across all axes. The midpoints of the stator face and magnet pairs were off by a vertical 0.027 inches; therefore, the height of the stator recess was brought down by 0.027 inches from 0.59 inches to 0.563 inches accordingly (Figures 33 and 34). The lever could then rest horizontally when in equilibrium (no electromagnetic force applied).

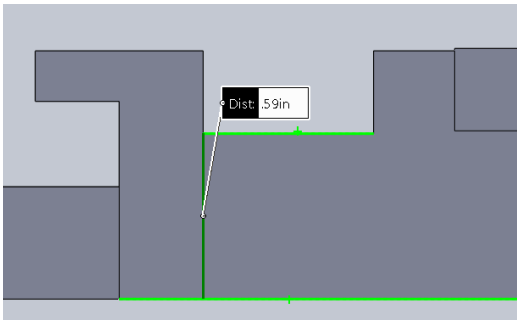

Figure 33: Original Distance Between Bottom of Motor Fixture and Bottom of Stator Recess

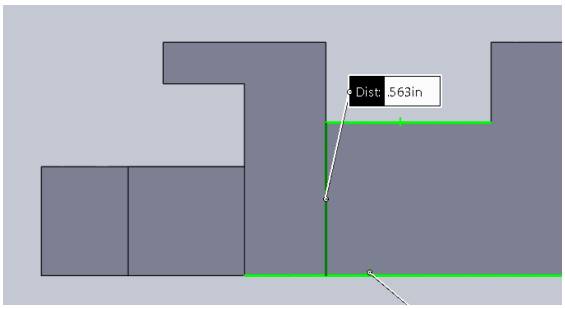

Figure 34: Updated Distance Between Bottom of Motor Fixture and Bottom of Stator Recess

The following factors were also observed as requiring design changes as to improve the functionality and rigidity of the motor assembly:

5. Enclosure mounting brackets did not have enough material at their base. One bracket arm snapped while removing supports from the PLA print.

6. Stand-alone clamp flanges remained too thin to stay rigid when bolt forces were applied; they still supplied sufficient clamping force, however, were exposed to high amounts of stress.

7. Flanges on motor fixture where clamp flanges attach was too thin at the base and began to yield over time. Deformities in the material were spotted in this area when the stator clamps were fully tightened.

8. Recess for stators did not place stators at center of magnet pairs when lever is horizontal. This was noticed during the editing of the Solid works file and made it so that force was not maximized between the magnets and stators.

We continued redesigning parts of the motor assembly, starting with the enclosure mounting brackets. One of these has snapped of while we were removing the supports from the 3D print, suggesting that the material around the base of the enclosure brackets was insufficient. We created multiple extrusions in SolidWorks to fill in the areas circled in red (Figure 35), creating a more solid profile for the enclosure brackets (Figure 36). This made the brackets much more rigid and difficult to flex in any direction.

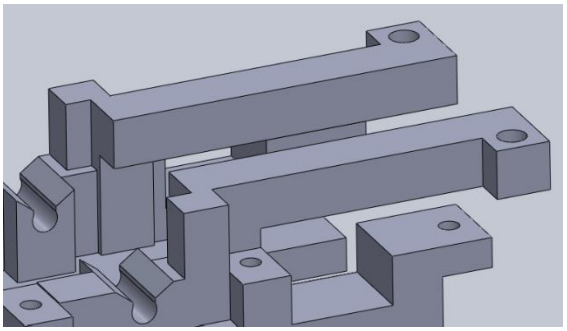

Figure 35: Original Motor Fixture Enclosure Bracket

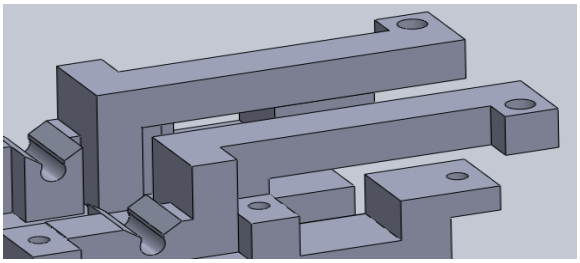

Figure 36: Updated Motor Fixture Enclosure Bracket

We then addressed the clamp flanges, which were yielding significantly under the applied bolt forces. This was created a similar problem to what we saw originally when the clamp flanges were bowing over the stators. This was resolved by increasing the thickness of the flanges from 0.16 inches to 0.25 inches (figures 37 and 38).

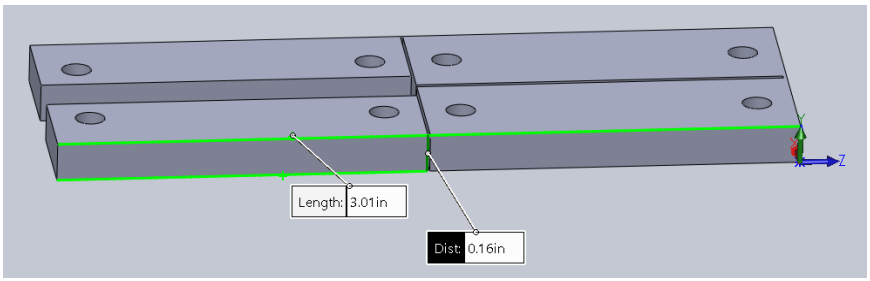

Figure 37: Original Thickness of Stand-Alone Clamp Flanges – 0.16 inches

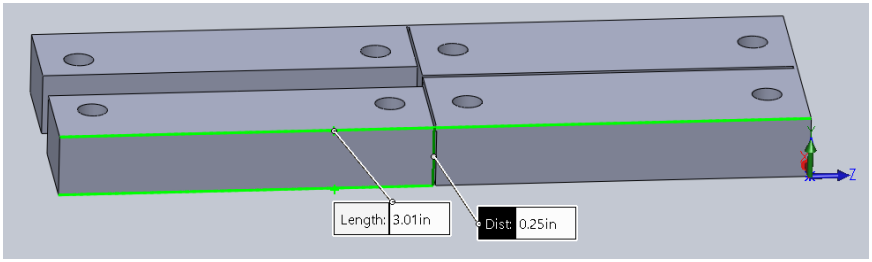

Figure 38: Updated Thickness of Stand-Alone Clamp Flanges – 0.25 inches

Additionally, the flanges on the motor fixture that the clamp flanges fasten too had proved to be too weak in our most recent assembly. After just a few hours of being assembled, the bases of the flanges began to crack, eventually breaking off due to the applied bolt forces. This was simply resolved by increasing the thickness of the base of all four flanges on the motor base by 0.1in. It proved to be an effective solution as the motor fixture flanges no longer showed signs of excessive stress or creep upon reassembly. Figure 39 shows the original dimensions of the motor fixture flanges while Figure 40 shows the updated dimensions.

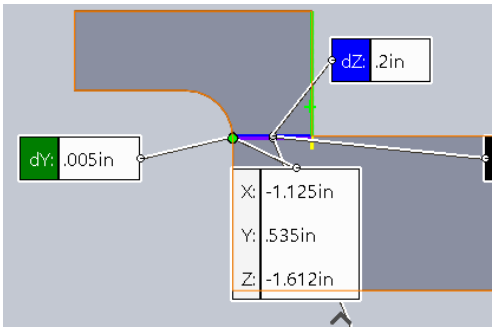

Figure 39: Original Dimensions of Motor Fixture Flanges

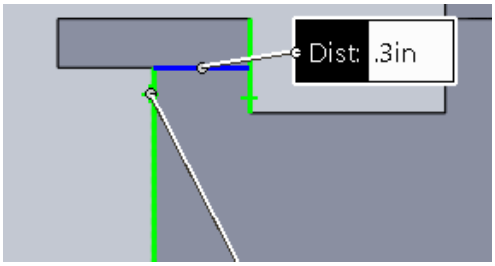

Figure 40: Updated Dimensions of Motor Fixture Flanges

A final physical assembly of the motor can be seen in Figure 41. Instructions on how to assemble the motor assembly can be found in Appendix A.

Figure 41: Final Motor Assembly

2.3 Motor Assembly SolidWorks Model

Once the physical motor assembly was built, we recreated the existing SolidWorks model of the final design for last year's project. Our goal was to create this assembly with parts representing the exact geometry and dimensions of the physical model so that easy measurements could be made for future iterations or replacement of parts. This required the creation of many new parts in SolidWorks.

Last year's motor assembly in SolidWorks utilized non-flanged bearings which did not accurately represent the true bearings reused in the current motor assembly or the spacing between bearings and motor fixture (Figure 42). A new part file was created modeling the actual bearings being used within the system (Figure 43). The dimensions of the bearings were found using a dial caliper. The SolidWorks part for the bearing was saved as: "Bearing.SLDPRT."

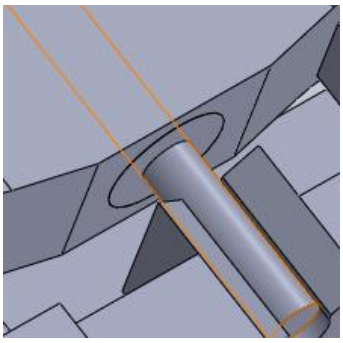

Figure 42: Non-Fanged Bearings in Last Year's SolidWorks Motor Assembly

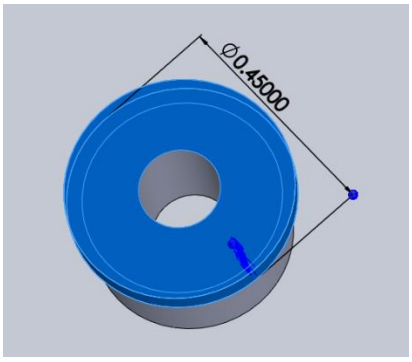

Figure 43: Updated Flanged Bearing SolidWorks Part

Last year's motor assembly in SolidWorks also used an odd sized axle that wasn't representative of the actual axle dimensions being used. A new axle part was designed in SolidWorks (Figure 44); its dimensions were determined by using a dial caliper to measure the physical axle within the system. The file for the new part was saved as: "New Pin.SLDPRT."

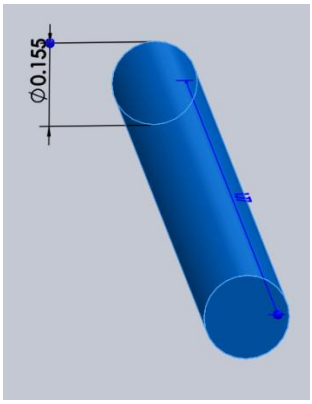

Figure 44: New Axle Part in SolidWorks

Additionally, the previous year's motor assembly did not include parts for the magnets in the lever arm. The magnets in the system were measured using a dial caliper and a part was created in SolidWorks (Figure 45). The part file was saved as: "Magnet.SLDPRT."

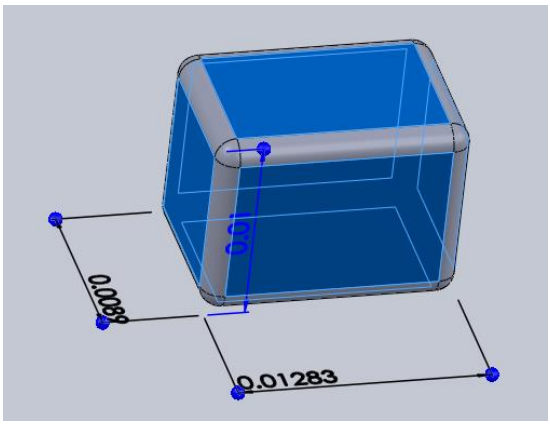

Figure 45: New Magnet Part SolidWorks

Since the new motor fixture saw separate clamp flanges implemented and a new fastening point on each clamp flange, a longer M3 bolt needed to be designed in SolidWorks so that a complete assembly could be built (Figure 46). This bolt was designed 1.1875 inches in length without threads since that is outside of the scope of this project. The SolidWorks file was saved as: "m3 1.1875 Hex Screw.SLPRT."

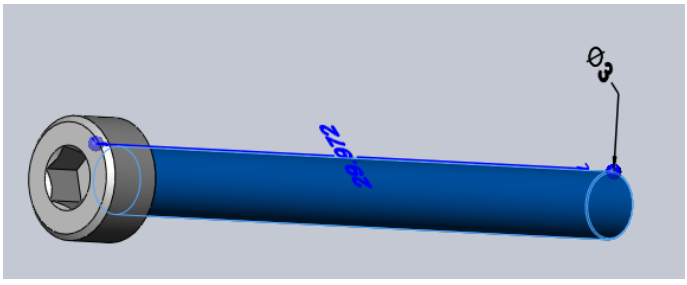

Figure 46: M3 1.1875in. Bolt in SolidWorks

These new parts, along with the existing motor fixture, lever, clamp flanges and bolts were assembled in SolidWorks and titled “2022 Motor Assembly 1.01” (Figure 47).

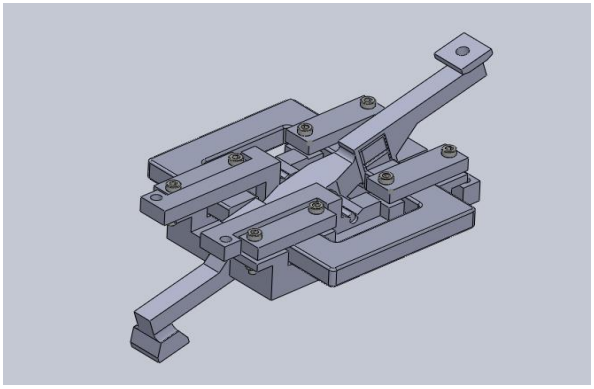

Figure 47: SolidWorks Assembly “2022 Motor Assembly 1.01”

2.4 Motor Assembly Force Testing

Once the new motor assembly had been reassembled, the output force of the lever was measured using a strain gage and an HX711 load cell. Using equipment found in Professor Stabile’s office, the strain gage circuit was created with a 9V battery as a power supply and a small potentiometer used to adjust the resistance of the circuit. An Arduino microcontroller was used to calibrate and read the strain gage, and the script used in the “Arduino” software is provided in Appendix B. Figure 48 shows the original strain gage circuit.

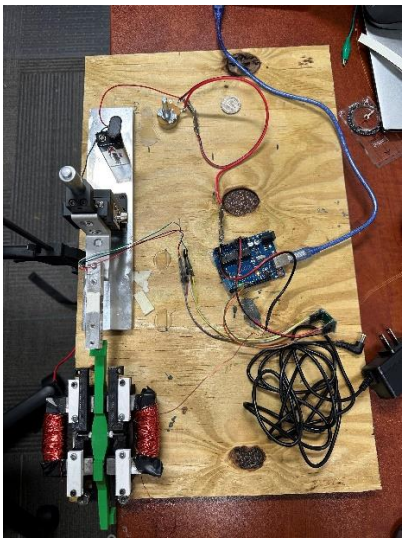

Figure 48: Original Strain Gage Setup

Before this circuit was even used to measure force of the lever arm, we encountered issues with dead 9V batteries and a possibly fried potentiometer, as almost no actuation was occurring to the lever arm. To resolve this, the 9V power supply was replaced with a 24V power supply, and the potentiometer was replaced with a larger 10 Ohm 100 Watt rotary rheostat. This circuit can be seen in Figure 49.

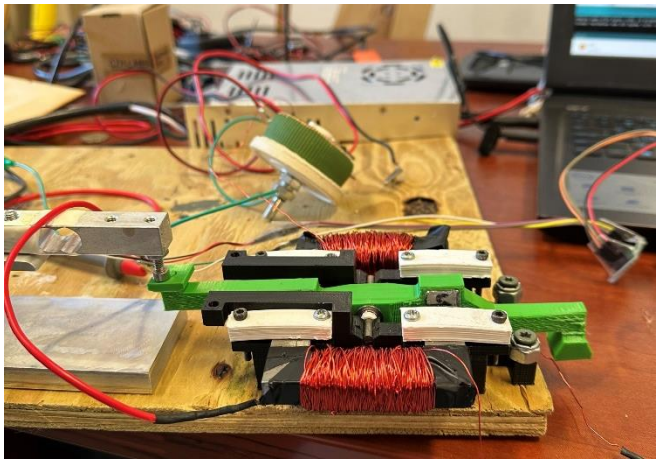

Figure 49: Motor Assembly (Front), Rheostat (Middle), 24V Power Supply (Back)

Given that the motor assembly was designed to accommodate a maximum deflection angle of 8 degrees, we chose to evaluate its force output at the cones for a 0-, 2-, 4- and 6-degree deflection angles. These angles provide 0-8 millimeters of cone movement, which is enough to cover the expected range of motion required to drive sound (at least 5 millimeters).

Before testing, the RX711 was calibrated using the Arduino script and an electronic balance. A mass was chosen and measured to be 286 grams on the balance (Figure 50). When this weight was placed on the strain gage, the Arduino script reported the mass at about 276 grams (Figure 51).

Figure 50: Mass Measuring 286 Grams on Electronic Balance

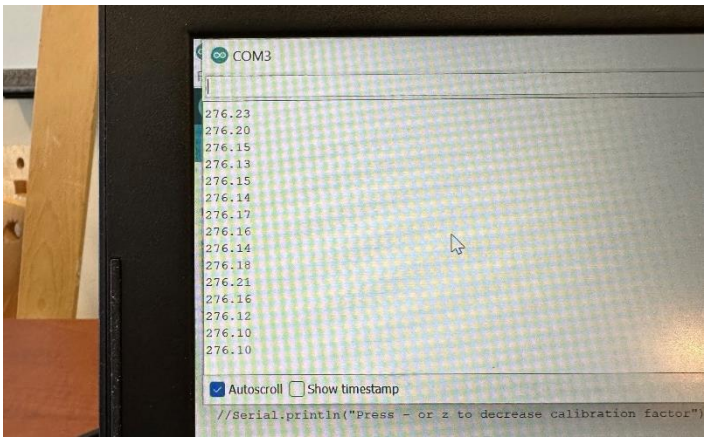

Figure 51: Arduino Script Registering Mass as 276 Grams

To correct this, the "calibration factor" in the provided Arduino script was edited from "820" to "845," (Figure 52) resulting in the script reporting the mass at about 286 grams (Figure 53).

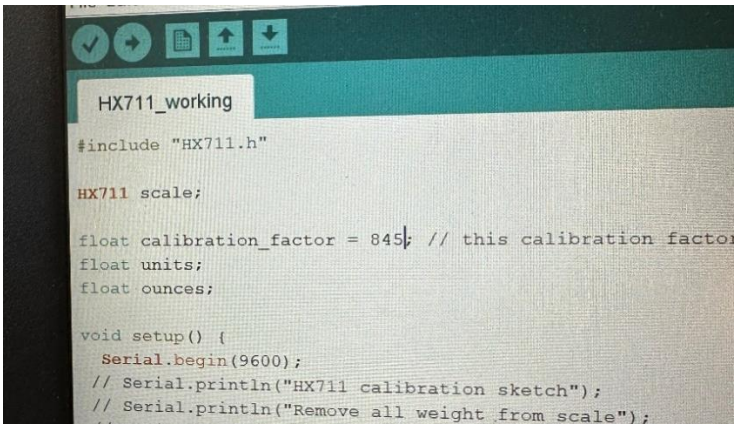

Figure 52: Editing Calibration Factor

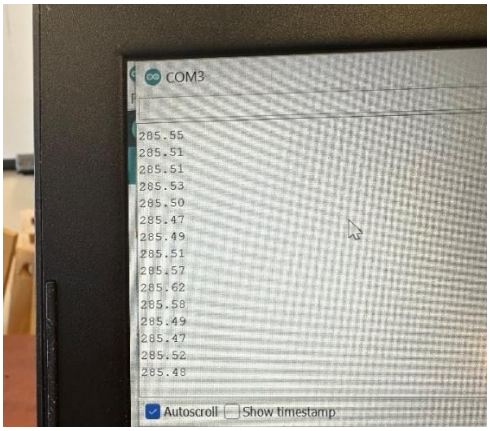

Figure 53: Mass Registering at 286 Grams in Arduino

With the strain gage calibrated, we began our trials. For each trial, the RX711 was adjusted so that its probe rested on the end of the motor assembly's lever arm when the lever was positioned at the deflection angle under test. The adjustment knob on the rheostat was oscillated while it and the motor assembly were powered by the 24V source. The software "Arduino" and provided script were then used produce graphs with the y-axis representing force (grams), and the x-axis representing time. The peaks of the graphs represent 3.12 amps through the motor (rheostat fully opened) while the trough represents 0 amps (rheostat fully closed). Figures 54-57 show the motor assembly in the strain gage fixture for deflection angles 0, 2, 4 and 6 degrees, while Figures 58-61 show the resulting force vs. time graphs for those respective deflection angles.

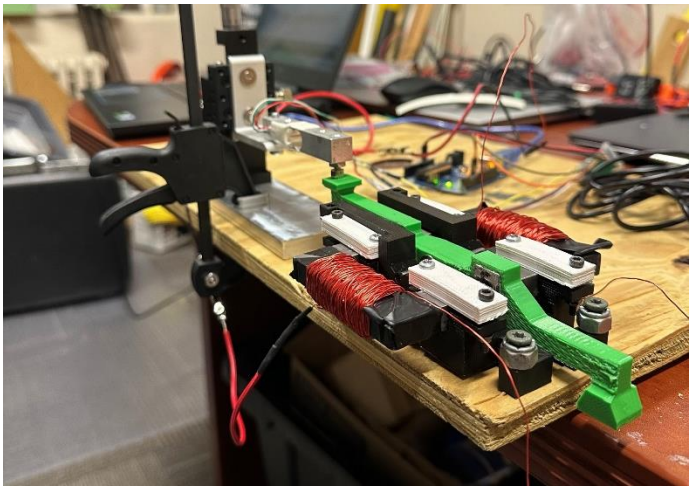

Figure 54: Motor Assembly in Strain Gage Fixture at Zero Degree Deflection Angle

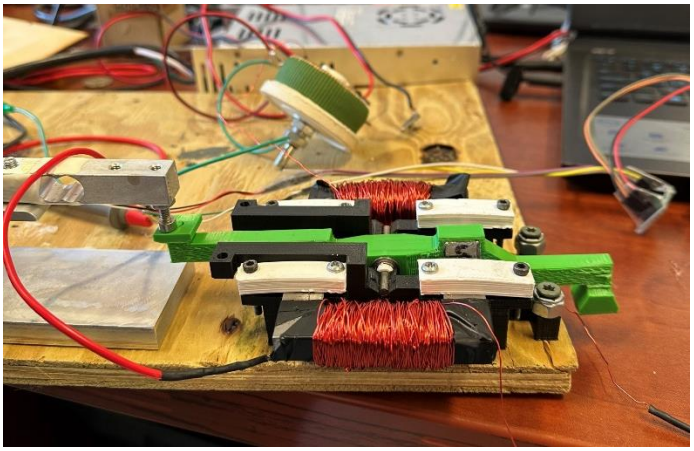

Figure 55: Motor Assembly in Strain Gage Fixture at Two Degree Deflection Angle

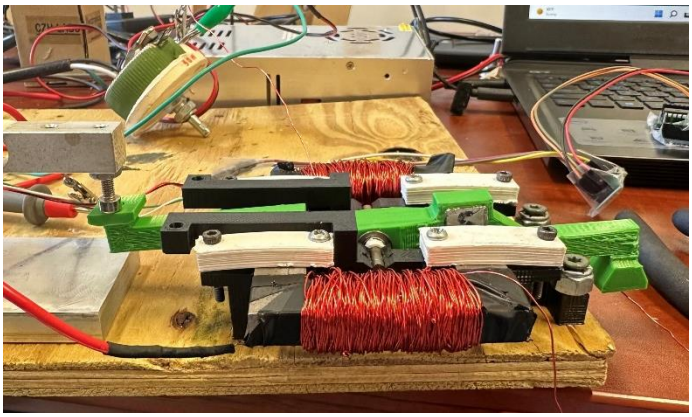

Figure 56: Motor Assembly in Strain Gage Fixture at Four Degree Deflection Angle

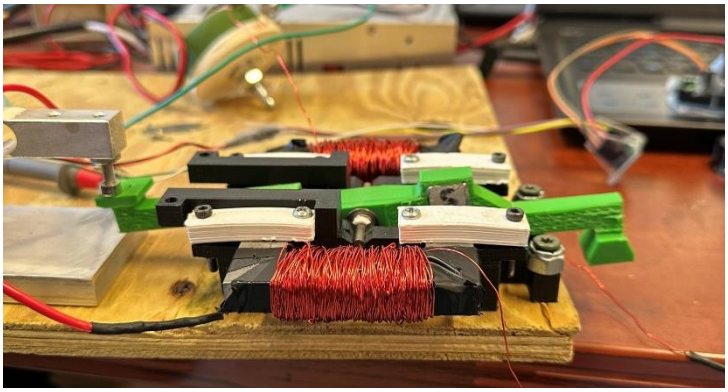

Figure 57: Motor Assembly in Strain Gage Fixture at Six Degree Deflection Angle

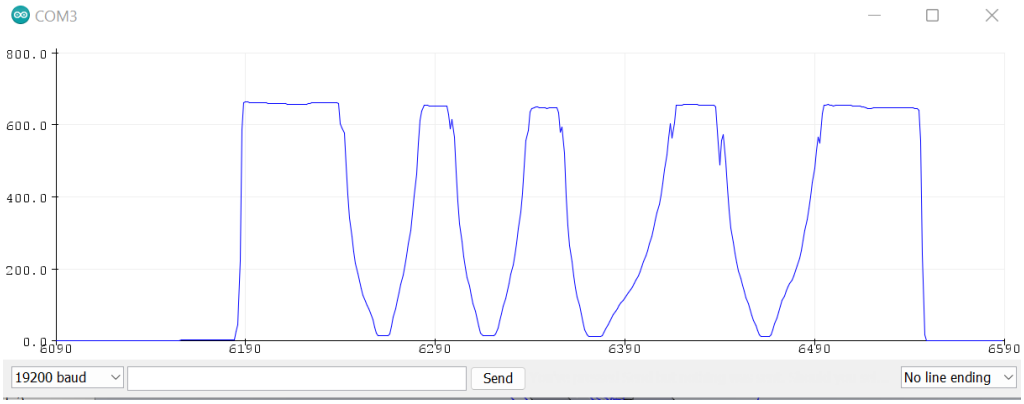

Figure 58: Force vs. Time Graph for Zero Degree Deflection Angle

Figure 59: Force vs. Time Graph for Two Degree Deflection Angle

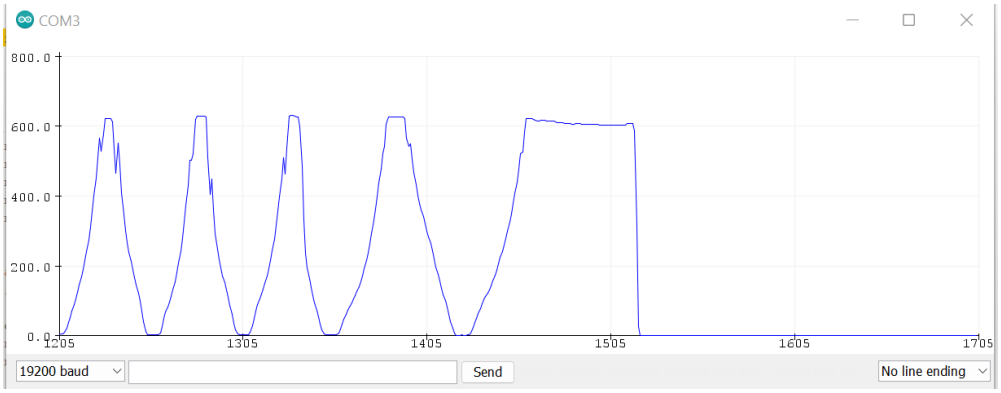

Figure 60: Force vs. Time Graph for Four Degree Deflection Angle

Figure 61: Force vs. Time Graph for Six Degree Deflection Angle

Electromagnetic force and current are in a linear relationship (Storr, 2022). Therefore, linear functions displaying force vs. current at the lever were generated for each deflection angle using the equation f(X)= ((Maximum Force-Minimum Force)/ (Maximum Current-Minimum Current)) *X. Values for maximum and minimum current were retrieved from the multimeter attached in series within the strain gage circuit while values for maximum and minimum force were taking from Figures 58-61. The functions of force vs. current for each deflection angle are shown in Figure 62. In this case, the maximum current allowed by the rheostat was 3.12 amps,

and the minimum current was 0 amps. The maximum forces at the lever for 0, 2, 4 and 6 degrees of deflection were 660 grams, 615 grams, 610 grams and 595 grams respectively. These force values can be used in conjunction with the air stiffness of the final enclosure to determine if the motor will sufficiently drive the cones.

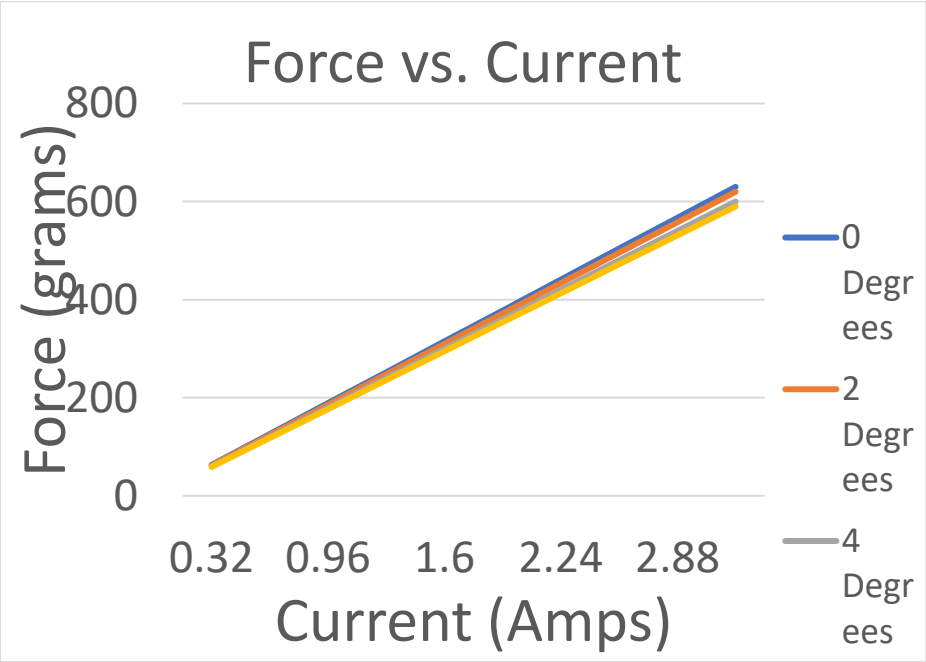

Figure 62: Force vs Current Graph for Each Deflection Angle

2.5 Improving the Strain Gage Circuit

As seen in Figure 49, the updated strain gage setup had no fixture to hold the rheostat. To adjust the current entering the motor assembly, the rheostat had to be held by hand and its resistance had to be adjusted with a pair of pliers. This test station proved to be very inefficient because low thermal efficiency of the rheostat would cause it to quickly heat up and make holding it unmanageable for the operator. The lack of a proper fixture for the rheostat also proposed risks of the rheostat accidentally touching and shorting out against metal components. To address these issues noted on the previous slide, an L-bracket fixture was designed on SolidWorks (Figure 63). This bracket was created so that the rheostat could be mounted safely away from the other electrical components in the strain gage setup. Additionally, this would eliminate the need to hold the rheostat by hand, therefore increasing the amount of time the test setup can be operated. The L-bracket was printed, and the rheostat mounted with a turn dial to eliminate the need to adjust the rheostats resistance with pliers (Figure 64).

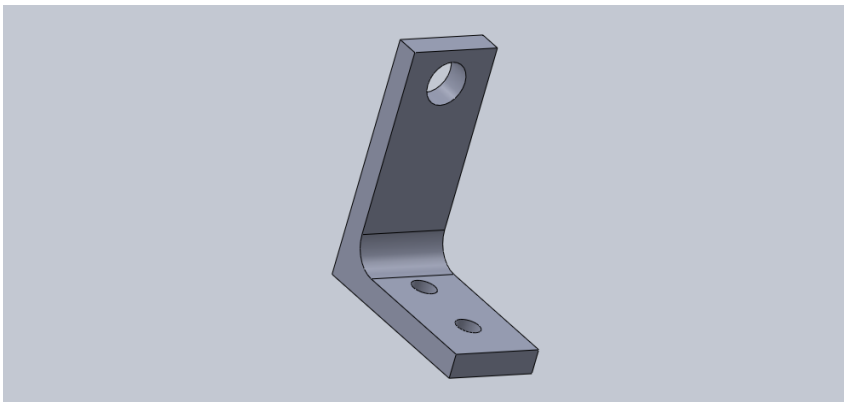

Figure 63: L-Bracket SolidWorks Model

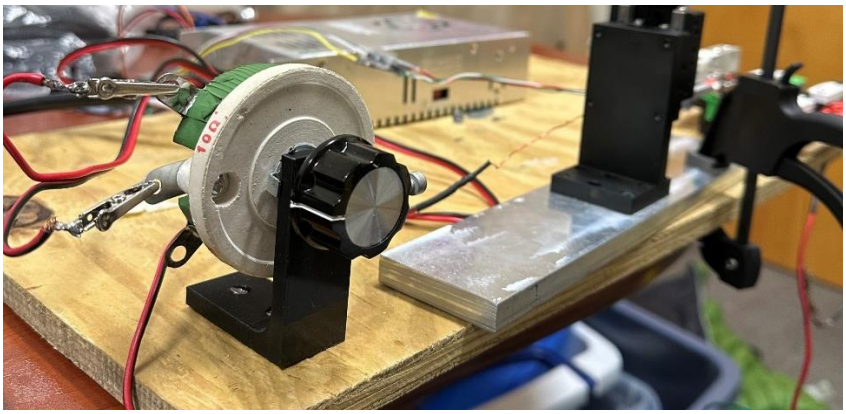

Figure 64: Mounted Rheostat with Turn Dial

We soon determined that although the rheostat had been properly fixtured and no longer provided complications from having to hold it by hand, it still was not an ideal regulator for the motor assembly. This is because when testing force vs. current for different deflection angles, the temperature of the rheostat would still increase significantly, which would add thermal resistance and cause the maximum current output by the rheostat to decrease over time. This resulted in Figure 61 being a non-representative comparison of deflection angles since each deflection angle was tested at a different maximum current. While the difference in max current between the time the rheostat was powered (Figure 65) and the time testing was completed (Figure 66) was only around 0.1 amps, it still resulted in some inaccuracy for data comparison.

Figure 65: Current Through Strain Gage Circuit at Time Rheostat was Connected

Figure 66: Current Through Strain Gage Circuit at Time Rheostat was Disconnected (Around 15 Minutes after Figure 64 was Captured).

To address the issues imposed by the rheostat, a voltage regulator was integrated into the strain gage setup (Figure 67). This voltage regulator uses pulse width modulation to regulate the level of current entering the motor assembly. It is a switching regulator, so it has a much higher thermal efficiency than a regular such as the rheostat. Upon testing of the motor assembly using the voltage regulator, it was found that the maximum current output was 3.16 amps, 0.04 amps higher than the maximum current output received from the rheostat (Figure 68). While this is not a significant difference, the voltage regulator did not exhibit thermal loss over the course of testing, allowing for a more accurate comparison of force vs. current for different deflection angles. Instructions on how to assemble the strain gage circuit with the voltage regulator can be found in Appendix B.

Figure 67: Voltage Regulator in Strain Gage Circuit

Figure 68: Maximum Current Output from Voltage Regulator

3.0 Ethics

Many aspects of the Engineering Code of Ethics were employed throughout the duration of this Major Qualifying Project. The 1st Fundamental Canon was followed throughout each process of physically prototyping of the motor assembly, as the health and safety of others was always a top priority when using public workshops such as the WPI Makerspace. Additionally, this project remained within the scope of mechanical engineering by focusing on the developing the mechanical functions of the motor assembly rather than electrical, and therefore conformed to the 2nd Fundamental Canon. Fundamental Canon's 4, 5 and 6 were also observed through this project, as all members contributing to the project acted professionally, the work of previous efforts was credited, and the project was performed by members of a reputable Institute, respectively. Lastly, the 8th Fundamental Canon was considered during the 3D printing of all parts, as environmental footprints were decreased through use of biodegradable materials.

4.0 Recommendations

4.1 Recommendation 1

The tolerance between the lever axle and bearings used in this project was set by manufacturer specifications. The goal for this bearing-axle interface was to provide the least amount of tolerance possible in the scope of this project, however the final motor assembly is seen to exhibit a very minute amount of play at this interface. The play is not enough to cause a point of failure when the magnets and stators are aligned optimally, and therefore should not pose any issues with operability, however future projects should explore the use of a bearing-axle interface of even tighter tolerance to eliminate this play.

4.2 Recommendation 2

The electromagnetic stators themselves were not iterated much further throughout this project to increase overall force output. Rather, the physical assembly was iterated to provide proper mechanics and maximize available power. Therefore, future projects should continue improving the capability of the stators to deliver larger electromagnetic fields and produce greater forces.

Bibliography

Ahrens, Z., Bressette, M., & McQuade, T., Whitock, B. (2020). *Development of a Low-Profile Home Speaker System.* (Undergraduate Major Qualifying Project No. E-project-030520-142719). Retrieved from Worcester Polytechnic Institute Electronic Projects Collection:

Pance, A., Leong, C., & Johnson, M. E. (2014, August 19). *Moving magnet audio transducer*. (U.S. Patent NO. 8811648 B2). U.S. Patent and Trademark Office. https://patentimages.storage.googleapis.com/9e/c8/4b/56758e56bf9e76/US8811648.pdf

Roy, H., D'Agostino, S., & DiMestico, R. (2018). *Low Profile Home Speaker: Moving Magnet Transducer.* (Undergraduate Major Qualifying Project No. E-project-042418-231630). Retrieved from Worcester Polytechnic Institute Electronic Projects Collection:

Storr, W. (2022, October 27). *The Electromagnet*. Basic Electronics Tutorials. https://www.electronics-tutorials.ws/electromagnetism/electromagnets.html

Wykes, A. J. (2022, October 6). *How speakers work: The basics to start*. SoundGuys. https://www.soundguys.com/how-speakers-work-29860/

Appendices

Appendix A: How to Assemble the Motor Assembly

Before assembling the motor assembly, the following SolidWorks files must be printed:

1. 2022 2.03 Base.SLDPRT
2. Bearing.SLDPRT
3. Clamp Flanges 1.SLDPRT
4. Clamp Flange 2.SLDPRT
5. Spacer.SLDPRT
6. New Lever 1.01.SLDPRT

These files can be found in the Microsoft Teams folder created for this MQP. In addition to these files, four magnets, two stators, two bearings, and a lever axle must be acquired which conform to the dimensions seen in files “Magnet.SLDPRT,” “1 piece stator block_same cross section_0.375_longer[9544].SLDPRT,” “Bearing.SLDPRT,” and “New Pin.SLDPRT” respectively. Once these parts are acquired, the motor assembly can be configured as follows:

1. Install two flanged ball bearings into either side of the lever arm using a vice to hold the lever and a rubber mallet to tap the bearings in. There is an interference fit between the bearings and the recess in the lever, therefore tap the bearings in lightly to avoid creating stress fractures in the lever.
2. Using a compass to determine the direction of magnetic field on the four acquired magnets, assemble two pairs of the magnets. Install these magnets pairs into the lever arm as seen in Figure 4. Accomplish this using soft taps from a rubber mallet to avoid cracking the frame of the lever. Secure the magnets within the lever using super glue or epoxy.
3. Slide the lever axle through the lever bearings and position a spacer on either side of the axle. Position the spacers so that they are fully touching the bearings.
4. Place the lever arm in the center of the motor fixture with the axle resting above the top-down grooves where it is to be inserted. Flex the motor fixture slightly to create more space between the supports and the lever so that the spacers can fall into their designated locations. Using a screwdriver, press both sides of the axle into the snap fit.
5. Place 1mm shims on each magnet surface and install the stators into the motor fixture in the orientation shown in Figure 4.
6. Fasten the clamp flanges onto the motor fixture and secure the stators.
7. Remove the shims and ensure the lever arm actuates without interfering with the motor fixture. If there is interference, readjust the positions of the stators until the interference disappears while preserving minimum clearance.

Appendix B: How to Assemble the Strain Gage Circuit

To assemble the strain gage circuit to test the motor assembly, follow the below instructions:

1. Mount the motor assembly to a piece of plywood. Use decking screws to fasten the enclosure mounts to the plywood. Figure 69 shows where we mounted the motor assembly.

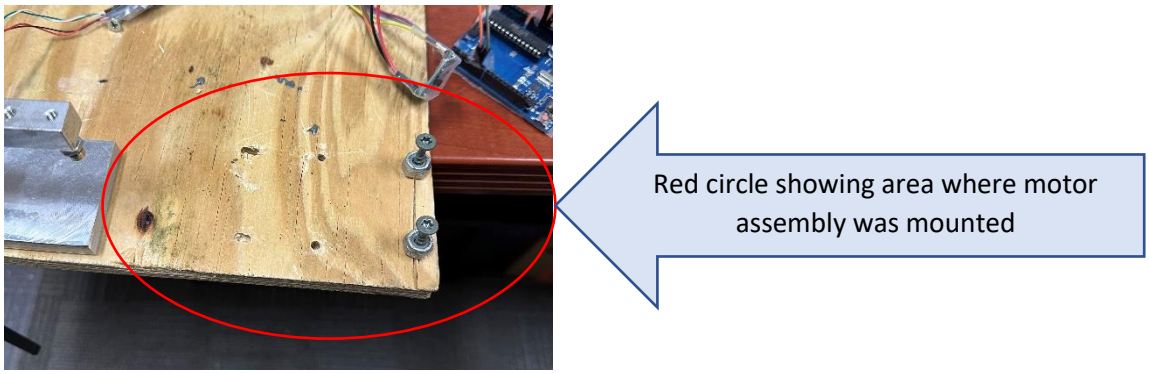

Figure 69: Area Where Motor Assembly was Mounted

2. Clamp the RX711 strain gage fixture to the plywood as seen in Figure 70.

Figure 70: Clamping the Strain Gage

3. Align the motor assembly's lever with the contact point on the RX711 strain gage. The adjustment knob seen on the strain gage can be used to adjust its height and position the lever at the desired deflection angle, as seen in Figures 54-57.
4. Plug in the 24V power supply to an outlet and connect it to the voltage regulator as seen in Figure 71.

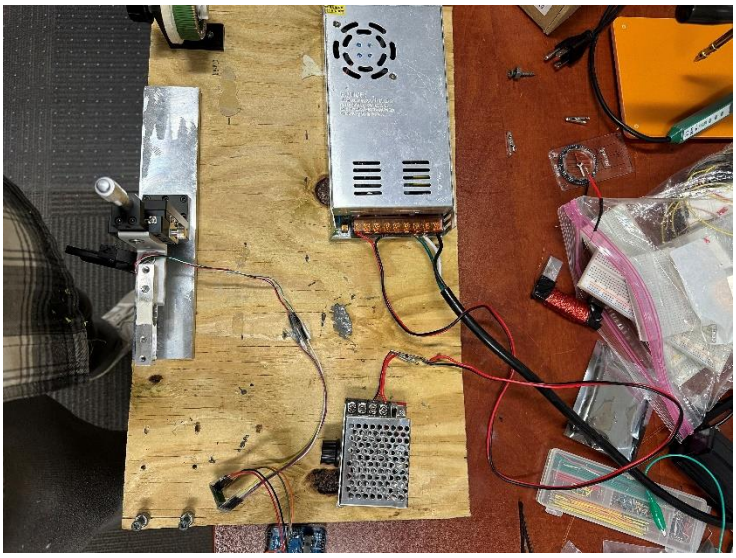

Figure 71: Connecting the Voltage Regulator to the Power Supply

5. Connect the leads of the motor assembly to the voltage regulator. The system can now be operated and the knob on the voltage regulator can be used to adjust the power received by the motor assembly. Figure 72 shows the positive and negative terminals on the voltage regulator where the motor is to be connected.

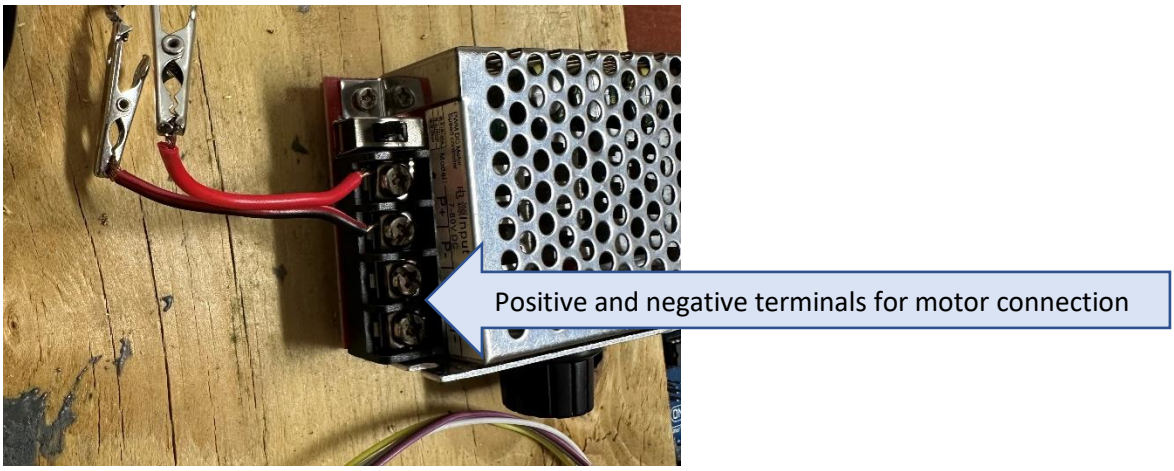

Figure 72: Connecting the Motor Assembly to the Voltage Regulator

6. Find the Arduino microcontroller attached to the strain gage and connect its USB to a computer. Open the software "Arduino" (this software can be downloaded online for free) and paste the code found in Table 1.

Table 1: RX711 Strain Gage Arduino Code

```
/*
 Setup your scale and start the sketch WITHOUT a weight on the scale
 Once readings are displayed place the weight on the scale
 Press +/- or a/z to adjust the calibration_factor until the output readings match the known weight
 Arduino pin 6 -> HX711 CLK
 Arduino pin 5 -> HX711 DOUT
 Arduino pin 5V -> HX711 VCC
 Arduino pin GND -> HX711 GND
*/

#include "HX711.h"

HX711 scale;

float calibration_factor = 845; // this calibration factor is adjusted according to my load cell
float units;
float ounces;

void setup() {
  Serial.begin(9600);
 // Serial.println("HX711 calibration sketch");
 // Serial.println("Remove all weight from scale");
 // Serial.println("After readings begin, place known weight on scale");
  //Serial.println("Press + or a to increase calibration factor");
  //Serial.println("Press - or z to decrease calibration factor");

scale.begin(5, 6);
  scale.set_scale();
  scale.tare();  //Reset the scale to 0

  long zero_factor = scale.read_average(); //Get a baseline reading
  //Serial.print("Zero factor: "); //This can be used to remove the need to tare the scale. Useful in permanent scale projects.
 // Serial.println(zero_factor);
}

void loop() {

  scale.set_scale(calibration_factor); //Adjust to this calibration factor

  //Serial.print("Reading: ");
  units = scale.get_units(), 10;
```

```
  if (units < 0)
  {
    units = 0.00;
  }
  ounces = units * 0.035274;
  Serial.print(units);
  //Serial.print(" grams");
  //Serial.print(" calibration_factor: ");
  //Serial.print(calibration_factor);
  Serial.println();

  if(Serial.available())
  {
    char temp = Serial.read();
    if(temp == '+' || temp == 'a')
      calibration_factor += 1;
    else if(temp == '-' || temp == 'z')
      calibration_factor -= 1;
  }
}
```

7. Once the code has been pasted into Arduino, press the “upload” button to program the microcontroller. Then, press “tools” and “serial plotter” to see a live chart of force versus time in grams.